Molecular Cell, Vol. 1, 421–431, February, 1998, Copyright ©1998 by Cell Press

Tumor Suppressor p16^{INK4A}: Determination of Solution Structure and Analyses of Its Interaction with Cyclin-Dependent Kinase 4

In-Ja L. Byeon, Junan Li, Karen Ericson, Thomas L. Selby, Anton Tevelev, Hee-Jung Kim, Paul O'Maille, and Ming-Daw Tsai*
Departments of Chemistry and Biochemistry
Campus Chemical Instrument Center
The Ohio State University
Columbus, Ohio 43210

Summary

The solution structure of the tumor suppressor p16^{INK4A} has been determined by NMR, and important recognition regions of both cdk4 and p16^{INK4A} have been identified. The tertiary structure of p16^{INK4A} contains four helix-turn-helix motifs linked by three loops. Twelve tumorigenic mutants of p16^{INK4A} have been constructed and analyzed for their structure and activity, and new mutants have been designed rationally. A fragment of 58 residues at the N terminus of cdk4 important for p16^{INK4A} binding has been identified. The importance of this region was further verified by mutational analysis of cdk4. These results and docking experiments have been used to assess possible modes of binding between p16^{INK4A} and cdk4.

Introduction

A negative regulator of the G_1-to-S transition, p16^{INK4A} (also called MTS1 or CDKN2), was discovered in 1993 by Beach (Serrano et al., 1993) and Skolnick (Kamb et al., 1994). Overexpression of p16^{INK4A}, hereafter abbreviated as p16, was shown to cause cell cycle arrest and to inhibit tumor cell proliferation in cell culture (Jin et al., 1995; Fueyo et al., 1996). This protein functions by inhibiting the activity of cyclin-dependent kinase 4 (cdk4) or cdk6. When inactive or inhibited, cdk4 and cdk6 cannot phosphorylate certain regulatory proteins, such as the retinoblastoma gene product (Rb). Phosphorylation of Rb triggers a series of events required for the G_1-to-S and G_0-to-S transitions in the cell cycle (Matsushime et al., 1992; Dyson, 1994; Kouzarides, 1995; Müller, 1995; Suzuki-Takahashi et al., 1995; Weinberg, 1995; Whyte, 1995). Thus, by inhibiting cdk4, functional p16 is capable of cell cycle arrest (Serrano et al., 1995). Inactivation of p16 by a variety of mechanisms may contribute to, or may even be the primary cause of, a variety of neoplasias (Shapiro et al., 1995; Serrano et al., 1996). Mutations in p16 have been found in >70 different types of tumor cells to date (for review, see Cordon-Cardo, 1995). It has also been reported that p16 itself can be inhibited by the Tax protein from human lymphocytic virus 1 (HTLV-1), which has been shown to be involved in the transcription machinery by binding to a variety of cellular proteins such as NF-κB and IκB (Hirai et al., 1994; Suzuki et al., 1996).

Figure 1 shows the primary sequence of p16, along with that of other proteins in the p16 family: p15, p18, and p19, both human and murine. P16 is comprised mainly of four ankyrin repeats, a structural motif about 33 amino acids long present in a variety of proteins in a diverse range of organisms. This motif is believed to be involved in protein–protein interactions (Lux et al., 1990; Greenwald and Rubin, 1992; Bork, 1993; Helps et al., 1995).

As described previously (Tevelev et al., 1996), p16 displays a strong tendency to aggregate at high concentration. This aggregation is often followed by denaturation of the protein as observed by NMR. Furthermore, the structure of p16 appears to be very flexible as demonstrated by rapid deuterium exchange of almost all protons during NMR studies in ^2H_2O. These two inherent properties of p16 have made the structural determination by NMR (and possibly X-ray) extremely difficult. Using NMR samples at concentrations as low as 0.2 mM, we completed the total assignment and determined the secondary structures of p16/Δ1–8 (a truncated form of p16, with the first 8 residues deleted). These results were the first structural analysis of an ankyrin repeat, and demonstrated that the repeat exists in helix-turn-helix structures (Tevelev et al., 1996). Subsequently, the structures of two other ankyrin proteins have been reported: 53BP2 (Gorina and Pavletich, 1996) and p19 (Luh et al., 1997).

Although p19 is a member of the p16 family, p16 and p15 are the only proven tumor suppressors in this family to date. While numerous studies have attempted to find mutations and/or deletions in the gene coding for p19 (Baghdassarian et al., 1996; Zariwala and Xiong, 1996; Miller et al., 1997), only one study has shown that p19 is altered, and this study showed that only 7% of the transcripts studied were aberrant (Baghdassarian et al., 1996). Moreover, while p16 plays a checkpoint function that demonstrates its role as a tumor suppressor, p18 and p19 appear to be more involved in the regulation of pre- and postnatal development (Zindy et al., 1997). In addition to such functional differences, p16 differs from p18 and p19 in certain structural properties: the conformational flexibility and the tendency to aggregate are significantly more severe for p16 than for p18 or p19. Another important point is that the p19 in the INK4 family mentioned above should not be confused with p19^{ARF}, which is a newly demonstrated tumor suppressor encoded by the same gene as p16 but in an alternative reading frame (Kamijo et al., 1997).

Although human cdk4 has been known for 10 years (Hanks, 1987), the mechanism of cdk inhibition by p16 has remained elusive due to the difficulty in obtaining structural information about cdk4. The structure of cdk2, which is 47% identical and 68% homologous to cdk4, has been solved in the free form and the complex with MgATP (De Bondt et al., 1993); furthermore, the structure of cdk2 complexed with cyclin A and a fragment of the inhibitor p27^{Kip1} has also been determined (Russo et

*To whom correspondence should be addressed (e-mail:Tsai.7@osu.edu).

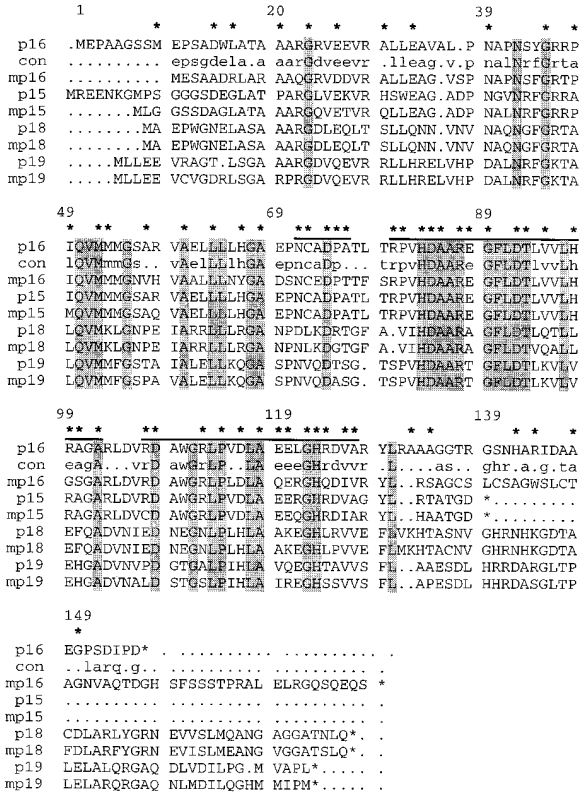

Figure 1. Sequences of the p16 Family

The sequences of human and murine (m) p16, p15, p18, and p19 and the consensus sequence (con). The absolutely conserved residues are shaded. The identity of p16 with p18 is 40%, and with p19 is 48%. The stars indicate the positions of mutations identified in tumor cells. The horizontal lines indicate the three regions with high frequencies of mutations. The sequences of the protein family members were obtained from the Swiss-Protein Database, with pileup and consensus sequence determined by Wisconsin Package version 9.1 of GCG (Oxford Molecular Group, Inc.).

al., 1996). One might hope that these structures can provide insight into the mechanism of p16–cdk4 interactions. However, the two systems are very different. The inhibitor $p27^{Kip1}$ belongs to the p21 family and shares no homology with p16. Additionally, although cdk4 and cdk2 are highly homologous, p16 inhibits cdk4 but not cdk2 (Sherr, 1996). Furthermore, while $p27^{Kip1}$ binds to both proteins of the cdk2–cyclin complex, p16 is known to bind to cdk4 both in the absence and presence of cyclin D (Zindy et al., 1997). Fåhraeus et al. (1996) has suggested that a 20-residue synthetic peptide of residues 84–103 of p16 is able to bind cdk4 and cdk6.

In this paper, we present the first high-resolution tertiary structure of p16 and use of the structure to analyze p16–cdk4 interactions. Some of the important residues for p16–cdk4 interactions have been identified for p16 (from structural and functional analyses of natural mutants) and cdk4 (from the yeast two-hybrid system followed by site-specific mutagenesis). The structural and functional information was then used to evaluate possible modes of binding between p16 and cdk4.

Results and Discussion

Determination of the Tertiary Structure

Our previous total assignment (Tevelev et al., 1996) used a truncated form (Δ1–8) of p16, which was expressed in *Escherichia coli* in insoluble form and renatured. In this work, we expressed full-length p16 as a glutathione S-transferase (GST) fusion protein in soluble form and removed the GST tag with thrombin. The sample conditions were the same as those in the previous work, except pH (7.5 instead of 7.0) and temperature (20°C instead of 27°C). Under these conditions, the "NMR lifetime" (the time before the protein aggregates and/or denatures) of p16 samples at low concentration (0.2–0.4 mM) improved from 1–2 weeks to 3–4 weeks. However, the structure is still highly flexible, as evidenced by the lack of nonexchangeable NH protons.

Despite the unfavorable conditions for NMR and the flexibility of the protein, a total of 1437 constraints (1370 distance and 67 dihedral angle) were obtained and used to generate an ensemble of 19 simulated annealing structures using the X-PLOR program (Nilges et al., 1988; Brünger, 1992). These structures converge and show good covalent geometry and good agreement with the constraints. Note that the constraints were obtained mainly from residues 14–134 because the first 13 and the last 22 residues of p16 show random structures. An ensemble of 19 structures are shown in Figure 2A. The structural statistics are summarized in Table 1.

Analysis and Discussion of the Structure

As shown in Figures 2B and 2C, the structure of p16 is characterized by a linear array of a repeating structure from four ankyrin repeats (I–IV). Each ankyrin repeat exhibits a helix-turn-helix (H-T-H) structure, except that the first half of the second ankyrin repeat consists of only one helical turn. The helices are designated as IA, IB, etc., and are packed into helix bundles. The four H-T-H motifs are connected by three loops designated as loop 1 (Ala-36 to Arg-46), loop 2 (Gly-67 to Arg-80), and loop 3 (Gly-101 to Leu-113). The orientations of the loops are such that they are perpendicular to the helical axes.

The key hydrophobic residues at the core of the helix bundles stabilize the bundle structures as shown in Figure 3A. Compared to the helix bundles, the loops show less defined structure due to conformational flexibility in these regions, making it difficult to derive detailed structural information for the loops. The highly conserved residue His-83 appears to stabilize loops 2 and 3. As shown in Figure 3A, the imidazole ring of His-83 is in proximity to the backbone protons of Thr-79 (from loop 2) and Val-106, Arg-107, Asp-108, and Leu-113 (from loop 3). Similar patterns of interactions have been observed for the ankyrin-repeat domain of the p53-binding protein 53BP2 (Gorina and Pavletich, 1996).

The solvent-accessible surface representation of p16 (Figure 3B) shows two important features: the presence of clusters of charged groups on the surface, and a pocket located on the right side of the representation. Both features could be important for the binding to cdk4.

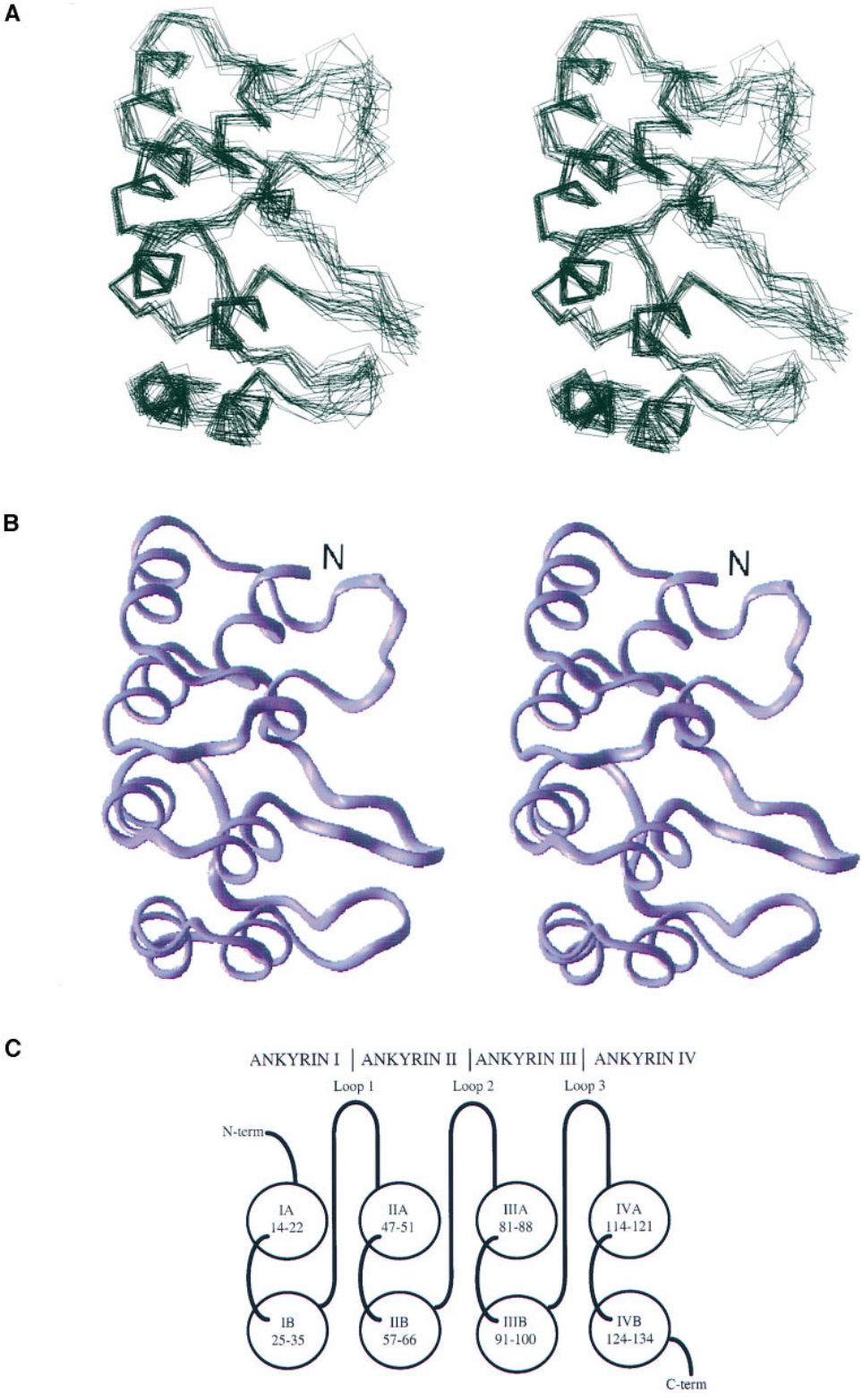

Figure 2. Solution Structure of p16

(A) Stereoview showing the best fit superposition of the α-carbon traces of residues 14–134 of the ensemble of 19 structures.
(B) Stereoview of a ribbon diagram of the p16 structure closest to the mean.
(C) Topology diagram of the p16 structure. Helices (in circle) are perpendicular to the plane of the page, and the residue numbers forming the helices are indicated.

Table 1. Structural Statistics for the Final 19 Structures of P16

Rms Deviations	<SA>
From experimental constraints:	
NOE distances (Å)	0.018 ± 0.001
Dihedral angles (°)	0.12 ± 0.05
From idealized geometry:	
Bonds (Å)	0.0021 ± 0.0001
Angles (°)	0.54 ± 0.01
Impropers (°)	0.35 ± 0.002
From the mean structure:	
Backbone heavy atoms for helices (Å)	0.58 ± 0.10
All heavy atoms for helices (Å)	1.06 ± 0.09
Backbone heavy atoms for residues 14–134 (Å)	0.95 ± 0.10
All heavy atoms for residues 14–134 (Å)	1.45 ± 0.13

[a] 1370 distance and 67 dihedral angle constraints were used.

The left inner wall of the pocket consists of a cluster of negatively charged groups that starts from Glu-88 on the left edge of the pocket and continues through Asp-84 and Gln-50 (which forms the back wall) to provide a polar region dominated by negatively charged side chains. The pocket is completed with the positively charged groups from Arg-46 and Arg-47 forming a right inner wall devoid of any negatively charged groups. The floor of the pocket begins with a protruding aromatic side chain from Trp-110 and continues (moving inward) with a polar threonine residue positioned such that the methyl group is oriented toward the indole ring and the hydroxyl group points upward toward the charged region of the pocket.

Comparison between p16 and p19 (Luh et al., 1997) structures indicates that they exist in similar global folds, except that p19 has an additional ankyrin repeat. Interactions involving this additional ankyrin repeat probably contribute to the additional conformational stability of p19. The antiparallel β-hairpin structure at the loops of the p19 structure was not detected in p16, possibly as a result of the conformational flexibility in the loop regions of p16. Detailed analyses of the structural differences between p16 and p19 could lead to understanding of the similarities and differences in their biological roles. It is also an interesting question whether the conformational flexibility of p16 makes it more feasible to locate and interact with cdk4.

Frequent Mutation Regions of p16

Some of the p16 mutations in tumor cells are deletions of one or more amino acid residues; these mutations are likely to grossly perturb the tertiary structure and thus the function of p16. Less clear are the properties of mutants with a single amino acid substitution. The sites of single amino acid mutations that have been identified in tumor cells to date are indicated by stars in Figure 1. Overall, few natural mutations occur in the flexible N- and C-terminal segments, implying that these regions do not contribute significantly to either the function or the structure of p16. Mutations have been noted with highest frequency in three regions: residues 71–76, 80–102, and 107–127. The first segment lies in loop 2; the second segment spans the entire ankyrin repeat III, and the third segment starts from loop 3 and ends at the beginning of helix IVB.

Functional Properties of Some Tumorigenic Mutants of p16

Although we have identified the frequently mutated structural regions of p16 in tumor cells, it is important to further investigate whether the natural mutants occurring in these regions actually lead to a decrease in p16 activity, and whether the decrease in activity is caused by structural changes. We therefore constructed 12 mutants, 9 of them from the three segments mentioned earlier, and analyzed them both structurally and functionally. The functional analysis was performed by in vitro cdk4 activity assay as shown in Figure 4 for wild-type p16 (A) and D84H (B). The IC_{50} values of the wild type and the mutants are presented in Table 2. All mutants showed decreased activities (increased IC_{50} values). The activities of the D84H, G101W, and H123Q mutants were undetectable and were the lowest among the mutants studied.

Structural Properties of Some Tumorigenic Mutants of p16

To determine if the decrease in activity is caused by structural changes, we further analyzed the mutants by NMR. The mutants N71S, H83N, H98R, G101W, P114L, and H123Q all displayed grossly broadened spectra, possibly due to a combination of structural perturbation and enhanced aggregation. Such spectra for G101W and P114L have been shown in our previous paper (Tevelev et al., 1996). These residues are likely to play structural roles. The mutants E26D, D84H, and D92A gave well-resolved, wild type–like proton NMR, but their tendency to aggregate was also increased, which prevented further structural analyses. Only the mutants H66Y, D84N, and R124H were stable enough for two-dimensional NMR analyses; NOESY spectra indicate that the conformations of these mutants are not significantly different from that of wild-type p16. It may be concluded, therefore, that these residues play important binding roles.

The conformational stability of p16 mutants was evaluated by guanidinium chloride (Gdn·HCl)–induced denaturation monitored by CD, based on a two-state model (Pace, 1986): $\Delta G_D = \Delta G_D^{H_2O} - m[\text{Gdn·HCl}]$. The free energy of denaturation $\Delta G_D^{H_2O}$ and the *m* values are listed in Table 2 for all mutants. N71S, H83N, D92A, H98R, G101W, P114L, and H123Q all show large differences in the *m* value relative to that of the wild-type p16. This difference can be attributed to different global conformations for the particular mutant or different mechanisms of unfolding/denaturation. Some mutants showing perturbed proton NMR properties also show perturbed denaturation behavior in guanidinium chloride–induced denaturation. The mutants E26D, D84H, D84N, and R124H have *m* values comparable to that of wild-type p16. Two of these mutants, D84N and R124H, show improved conformational stability.

The conformational perturbations in H83N, H98R, G101W, P114L, and H123Q can be explained on the basis of the p16 structure. As described earlier, His-83

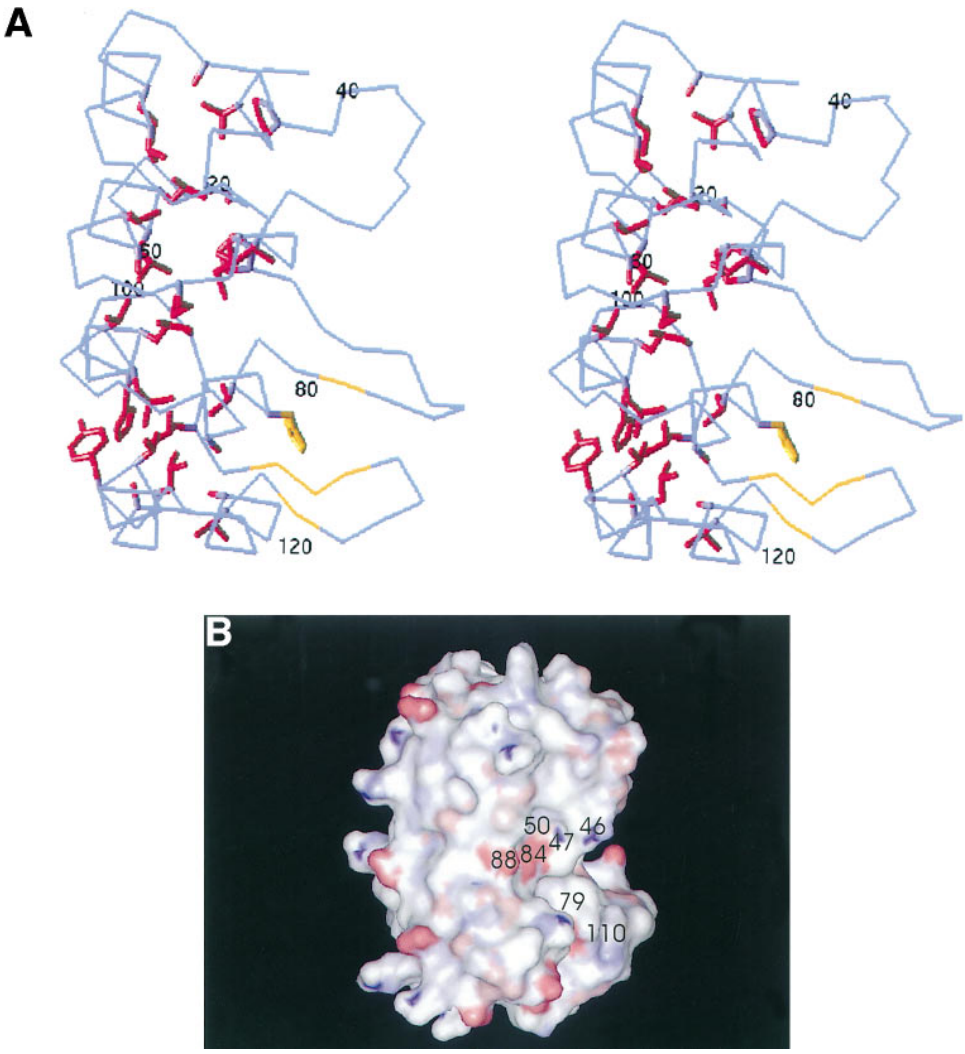

Figure 3. Important Side Chain Properties

(A) The important side chains that stabilize the helix bundle structures are shown in red. The backbone of the residues that interact with the His-83 imidazole ring are indicated in orange.

(B) Solvent-accessible surface representation of p16. Positive and negative charges are indicated by blue and red, respectively.

provides important stabilization between loops 2 and 3. His-98 (located in Helix IIIB) may interact with the side chains from Leu-94, Leu-104, Tyr-129, Leu-130, and Ala-133 and assists in stabilizing the helix bundle structure between ankyrins III and IV (see Figure 3A). The highly conserved Gly-101 is the initiating residue of loop 3, whereas the absolutely conserved Pro-114 is the initiating residue of helix IVA. Introduction of bulky side chains to these two residues could disturb the secondary structures. His-123, which is located in the turn between helix IVA and helix IVB, interacts with Gly-89 and Arg-87 backbone protons via the imidazole ring; these interactions stabilize the turn regions between ankyrins III and IV and keep the helices bundled together.

Rational Design of New p16 Mutants

The above results suggest that it is possible to predict, based on a specific amino acid position, whether other mutations of p16 found in cancer cells may lead to structural perturbations. Furthermore, we should be able to rationally design new mutants with impaired structure (and possibly also impaired activity). For example, structural analysis suggests that the side chain of Leu-78 stabilizes the interaction between loop 2 and loop 3 through hydrophobic interactions with the side chain of Ala-73, Val-106, and Ala-109. To verify that this residue is structurally important, we constructed L78A and showed that it aggregates severely and its proton NMR is very broad. Its function was also impaired: the IC_{50} value for the inhibition of cdk4 increases by 100-fold. It will be interesting to see whether this mutation affects cell cycle proliferation.

Identification of a p16-Binding Fragment of cdk4 Named C5

A cdk4 epitope library consisting of 7×10^4 independent clones was used to screen for p16-binding fragments

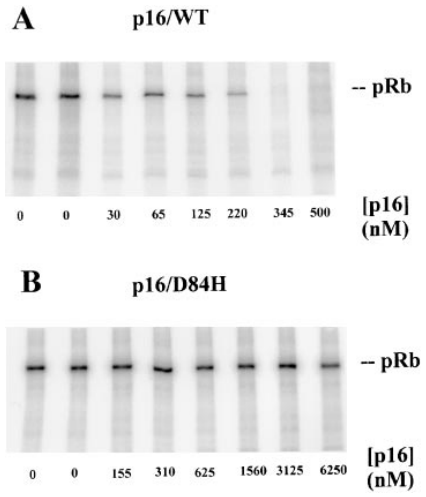

Figure 4. Assay of p16 Activity

Gels of in vitro phosphorylation of pRb by cdk4 in the presence of increasing concentrations of wild-type p16 (A) and D84H (B). Lanes 1 and 2 are negative controls.

by use of the yeast two-hybrid system. Binding of the proteins in these hybrids was measured by the liquid β-galactosidase assay. The shortest clone with p16-binding activity encompassed the first 58 N-terminal amino acids of cdk4 plus additional ATC CTA AAT nucleotides added at its N terminus and codons corresponding to amino acids 257–266 of cdk4 added to its C terminus. Removal of the extra amino acids from both termini did not affect p16 binding as demonstrated by the liquid β-galactosidase assay (data not shown). This minimal p16-binding fragment was named C5. The p16-binding activity of C5 was comparable to that of cdk4 and significantly above the background as measured by omitting C5 or by binding of C5 to lamine.

The ability of C5 to bind cdk4 was further verified by in vitro pull-down assays. Figure 5A shows the result of one of the pull-down assays with free C5 and S-tagged p16. Detection of the C5 band in lane 3 indicates binding between C5 and S-p16, while comparison between lanes 2 and 3 indicates that cotranslation is required for detection of binding. In addition, we further verified that C5 behaves similarly to cdk4 by showing that the R24C mutation, which is known to knock out the p16-binding activity of cdk4 (Wölfel et al., 1995), also partially impairs the p16-binding activity of C5 (Figures 5B and 5C). As another negative control experiment, we have shown that C5 also does not bind to an unrelated protein, GST (data not shown). Taken together, the results support that C5 binds to p16 specifically.

We do not suggest that C5 is an exclusive fragment for p16 binding, particularly since it shows a random coil structure in NMR analysis in the absence or presence of p16 (data not shown). It is not unreasonable that the C5–p16 complex can be detected in biological assays (which can detect a small percentage of the complex), but not under NMR conditions. However, identification of C5 allowed us to focus on this region to identify key p16-binding residues by mutagenic analyses of the full-length cdk4, as described in the next section.

Identification of Key p16-Binding Residues in cdk4

Nearly half of the residues in the first 58 amino acids of cdk4 were mutated and their p16 binding affinity assayed. Each single mutant of cdk4 was expressed in vitro and assayed for p16 binding using pull-down assays with S-p16. The wild-type cdk4 and its R24C mutant were used as positive and negative controls, respectively. The qualitative results are summarized in Table 3 (middle column). Of the 22 mutants studied, K22A, R24C (control), D25A, and L34D lost binding activity, while R5A and E56A showed weaker binding. Since these assays are only qualitative, the mutants showing negative binding were further examined by a complementary pull-down assay with S-tagged cdk4. As shown in the right column of Table 3, K22A, R24C, and L34D showed lack of binding in this assay, while D25A and E56A showed weak binding. Figure 6 shows part of the gels of these assays. Four mutants outside of the C5 region were also examined: H68A, T80A, K88A, and T172V, all of which showed normal p16-binding activity (data not shown).

Table 2. Activity and Conformational Stability of P16 Mutants

Mutant	IC_{50} (nM)	$\Delta G_D^{H_2O}$ (kcal/mol)	*m* (kcal/mol•M)
Wild type	70 ± 25	1.9 ± 0.05	2.9 ± 0.05
E26D	280 ± 52	1.1 ± 0.1	2.6 ± 0.1
H66Y	469 ± 96	1.4 ± 0.05	3.3 ± 0.05
N71S	250 ± 87	1.7 ± 0.08	1.7 ± 0.08
H83N	243 ± 37	1.6 ± 0.05	1.4 ± 0.04
D84H	>6000	1.6[b]	3.1[b]
D84N	4000 ± 900	2.9[b]	2.6[b]
D92A	850 ± 295	1.0 ± 0.03	1.3 ± 0.04
H98R	2125 ± 225	0.4 ± 0.1	1.6 ± 0.02
G101W	>6000	2.3[b]	1.8[b]
P114L	No activity detected[c]	2.2[b]	1.8[b]
H123Q	>6000	0.7 ± 0.02	6.9 ± 0.2
R124H	730 ± 230	2.6 ± 0.08	2.9 ± 0.09

[a] All data in this table were obtained for p16 with the first 8 residues truncated. All mutants have been identified in tumor cells, except D92A (but D92N does).

[b] Values from Tevelev et al. (1996).

[c] From Koh et al. (1995), Parry and Peters (1996), and Liu et al. (1995).

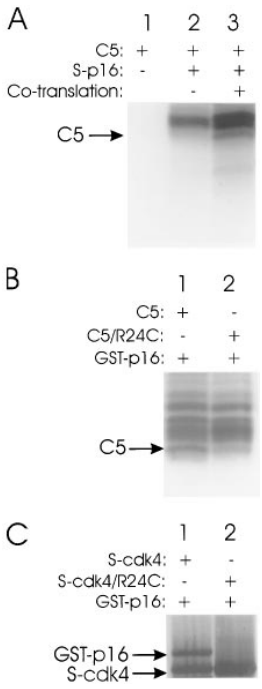

Figure 5. Binding of C5 and P16

(A) Binding between free C5 and S-tagged p16. The proteins were produced by in vitro translation and labeled with ^{35}S-methionine. Samples were loaded on S-protein agarose, which was subsequently washed followed by boiling in gel loading buffer. The eluants were separated by SDS–PAGE on a 15% tricine gel. Lane 1, C5 only (negative control); lane 2, S-p16 and C5, translated separately; lane 3, S-p16 and C5, cotranslated. The presence of the C5 band in lane 3 indicates binding of C5 to p16 when C5 and S-p16 are cotranslated. (B) Effect of R24C mutation on the binding of C5 to GST-p16. The binding of C5 to GST-fused p16 (lane 1) was compared to that of the R24C mutant of C5 (lane 2). Glutathione-Sepharose was used in the pull-down assay. In both cases, the proteins were cotranslated. The C5 band in lane 1, released from its complex with GST-p16, clearly is stronger than the R24C band in lane 2. The extra bands in (A) and (B) are unidentified proteins that are also labeled. (C) Positive control for the effect of R24C mutation on the binding of cdk4 to p16. Lane 1, GST-p16 and S-cdk4; lane 2, GST-16 and S-cdk4/R24C, translated separately. S-protein agarose was used in this pull-down assay. The band of GST-p16, released from its complex with S-tag-fused cdk4, appeared in lane 1 but not in lane 2.

Table 3. Effects of Point Mutations of Cdk4 on P16 Binding

cdk4 Point Mutation	p16-Binding Ability in Each System: cdk4/S-p16/ S-Protein Agarose	S-cdk4/GST-p16/ S-Protein Agarose
Wild type	+	+
R5A	Weak	+
Y6A	+	
E7A	No expression	
E11A	+	
Y17F	+	
V20T	+	
Y21A	+	
K22A	–	–
A23S	+	
R24C	–	–
D25A	–	Weak
H27A	+	
H30A	+	
V32T	+	
L34D	–	–
L34A	+	
K35A	+	
S36A	+	
R38A	+	
N41A	+	
R55A	+	
E56A	Weak	Weak

While our work was in progress, Coleman et al. (1997) also reported a series of cdk4 mutants involved in cyclin D1 and p16 binding. Some of the mutants in their work differ from ours; however, their main conclusion that "cyclin D1 and p16 binding sites are overlapping and are located primarily near the amino terminus" is in general agreement with our results.

Analyses of the Possible Nature of p16–cdk4 Interactions

Although a large number of mutants have been analyzed for both cdk4 and p16, only a limited number can be concluded to be important for binding between the two proteins. For p16, the majority of mutants are structural mutants and only residues His-66, Asp-84, Arg-124, and less certainly Glu-26 and Asp-92 are good candidates for cdk4-binding residues. For cdk4, only Lys-22, Arg-24, and less certainly, Asp-25, Leu-34, and Glu-56 are good candidates for p16-binding residues. Since most of these residues are charged residues, and since there are charged clusters on the surface of p16 as shown in Figure 3B, it is possible that electrostatic interactions between charged residues contribute significantly to the interaction between p16 and cdk4.

We further performed docking experiments to assess the possible binding modes between p16 and C5, using Global Range Molecular Matching (GRAMM) calculations (Katchalski-Katzir et al., 1992). The structure of C5 was constructed from the coordinates of cdk2. Calculations were completed for 1000 structures. As shown in Figure 7, the structure with the best energy score fits well with our functional results. The C5 peptide chain is aligned along the loop face of the p16 structure. The overall surface contact is primarily between loops 1 and 2 of p16 and the first two β strands of C5. Possible charge–charge interactions are described in the legend. These ionic interactions are interdispersed between stretches of hydrophobic amino acid residues on both proteins.

The actual binding mode could be different from that shown in Figure 7, particularly if the proteins undergo large conformational changes upon binding. However, since ankyrin repeats are important motifs in protein–protein interactions, it is quite possible that ankyrin repeat structures of p16 are directly involved in the binding to cdk4. The role of the helix bundle could be to hold the loops in position, and the flexibility of the loops could allow for possible conformational changes needed for binding. This concept is different from the proposal by Luh et al. (1997) that the face of the second helices of the ankyrin repeats might be the site of interaction with the kinase. In any case, the binding model depicted in Figure 7 provides a reasonable "working model" for us to design further experiments to elucidate the nature

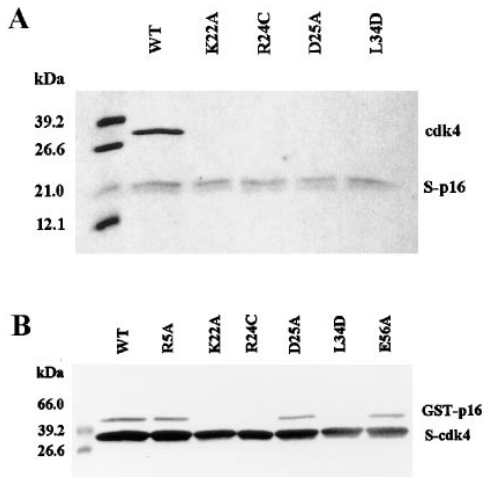

Figure 6. Assay of p16 Binding to Cdk4 Mutants

(A) Wild type and mutants of cdk4 were in vitro expressed and incubated with in vitro expressed S-tagged p16. Each mixture was loaded on an S-protein agarose column. Unbound proteins were washed out from the column. Bound proteins were eluted by boiling in SDS-gel loading buffer and separated on a 12% SDS–polyacrylamide gel.

(B) Wild type and mutants of S-tagged cdk4 were in vitro expressed and incubated with in vitro expressed GST-p16. Each mixture was loaded on an S-protein agarose column and separated as described in (A).

of p16–cdk4 interactions. Several other binding modes with slighly lower energy scores, including ones binding to the helical side of p16, will also be considered.

Experimental Procedures

Expression and Purification of p16

Human p16 was expressed in soluble form as a glutathione S-transferase (GST) fusion protein in *E. coli* BL21 (DE3) (Novagen). The cell lysate was purified on a glutathione-agarose column; p16 was cleaved from the column with thrombin and further purified by an S-100 column equilibrated with 4 mM HEPES buffer containing 1 mM DTT and 5 mM EDTA (pH 7.5).

NMR Experiments and Structural Determination

All NMR experiments were performed on a Bruker DMX-600. Both ^{15}N and $^{15}N,^{13}C$ uniformly labeled proteins were used; protein concentrations used varied from 0.2 to 0.4 mM. The distance restraints for the p16 structure calculations were obtained from the following NOE data (t_m = 100 or 150 msec): 2-D NOESY, 3-D ^{15}N-edited NOESY-HSQC (Marion et al, 1989; Sklenar et al., 1993), 3-D ^{13}C-edited NOESY-HMQC (Fesik and Zuiderweg, 1988), 3-D simultaneous $^{15}N/^{13}C$-edited NOESY (Sattler et al., 1995), 4-D $^{15}N/^{13}C$-edited NOESY (Muhandiram et al., 1993) and 4-D $^{13}C/^{13}C$-edited NOESY (Vuister et al., 1993). The φ torsion angle restraints were obtained from 3-D HNHA (Kuboniwa et al., 1994), and the side chain χ^1 torsion angles from 2-D TOCSY (Bax and Davis, 1985) in ^2H_2O and the 3-D NOESY data mentioned above. The NMR data were processed using XWINNMR (Bruker) and Felix (Molecular Simulations, Inc.). Structures were calculated on Silicon Graphics O2 workstations or a Cray T90 Supercomputer using a simulated annealing method (Nilges et al., 1988) with the X-PLOR program (Brünger, 1992). The structural images were generated using Insight II (Molecular Simulations, Inc.) or MOLMOL (Karadi et al., 1996).

Construction of Baculovirus-Expressing cdk4 and Cyclin D2

Human cdk4 cDNA was obtained by RT–PCR from total RNA of HeLa cells. The cdk4 cDNA was subcloned into BamHI and EcoRI sites of the pBacPAK8 phagemid (Clonetech) using primers that resulted in pBAC/cdk4 transfer vector. The C-terminal primer encoded six histidines fused to cdk4. The cDNA for cyclin D2 was subcloned by PCR into EcoRI and BglII sites of pBacPAK8 using template human cyclin D2 cDNA, which yielded pBAC/clnD2 transfer vector. Baculovirus was constructed using Autographa Californica nuclear polyhedrosis virus BacPAK6/Bsu36I DNA and Spodoptera frugiperda Sf-9 cells following the manufacturer's instructions (Clontech).

Production and Purification of cdk4/Cyclin D2 holoenzyme

The cdk4/cyclin D2 complex was purified from HighFive cells (Invitrogen) by modifying a published procedure (Koh et al., 1995). Cells were resuspended in buffer A (20 mM Tris–HCl [pH 7.5 at room temperature], 100 mM NaCl, 0.1 mM Na_3VO_4, 1 mM NaF, 10 mM β-glycerophosphate, 5 mM β-mercaptoethanol, 0.2 mM AEBSF, 5 mg/ml aprotinin, 5 mg/ml leupeptin). Lysates were cleared by centrifugation and loaded on a TALON (Clontech) resin column. After washing the column with buffer A, then buffer A containing 10 mM imidazole, the cdk4/cyclin D2 holoenzyme was eluted in buffer A with 50

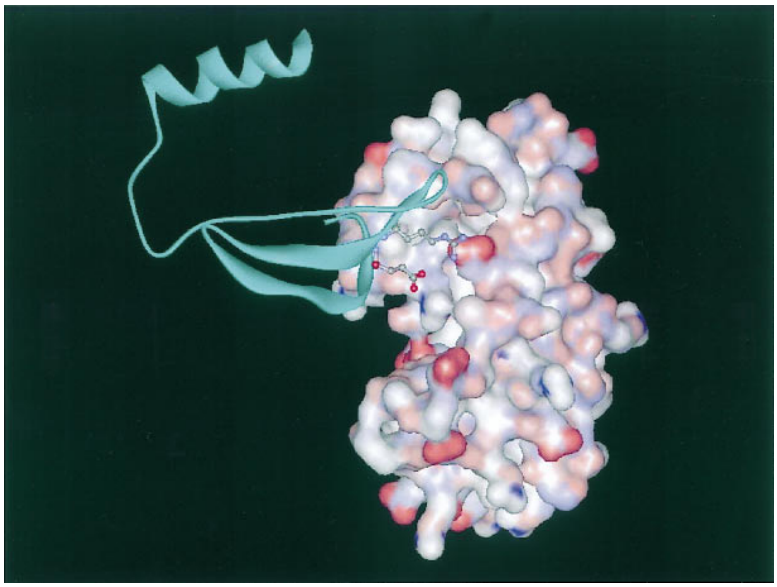

Figure 7. Working Model for the C5–p16 Complex

The model is depicted such that the ionic interactions between specific charged residues are visible. Side chains of Arg-24 and Glu-7 of C5 (blue ribbon) are shown in ball-and-stick mode. The p16 residue facing C5/Arg-24 is Glu-69, and that facing C5/Glu-7 is Arg-47. C5/Lys-22 could interact with p16/Asp-74. The p16 structure shown is 140° rotated from that in Figure 3B.

mM imidazole, dialyzed against Kinase buffer (50 mM HEPES [pH 7.5], 10 mM $MgCl_2$, 2.5 mM EGTA, 0.1 mM Na_3VO_4, 1 mM NaF, 10 mM β-glycerophosphate, 1 mM DTT), and concentrated to approximately 0.3 mg/ml. AEBSF, leupeptin, and aprotinin were added to the same concentrations as in buffer A. Aliquots were stored at −80°C.

Assay for cdk4 Inhibition

The in vitro cdk4 inhibition assay (Serrano, et al., 1993; Hannon and Beach, 1994) involved 3–10 units of the cdk4/cyclin D2 complex and varying concentrations of p16 or mutant in Kinase buffer supplemented with 0.2 mM AEBSF, 2.5 mg/ml leupeptin, and 2.5 mg/ml aprotinin in a total volume of 15 μl. These were preincubated for 30 min at 30°C. GST-Rb (50 ng) and 2 μCi of [γ-^{32}P]-ATP were added, and the samples were incubated for an additional 15 min at 30°C. *E. coli* BL21(DE3) harboring the plasmid pGEX (Pharmacia Biotech) containing human "large pocket" Rb cDNA corresponding to Rb amino acids 379–928 were grown, and the GST-Rb protein was purified following a published procedure (Meijer and Kim 1997). The cdk4 activity was determined by the radioactive phosphate incorporation into substrate Rb. The IC_{50} value is the amount of p16 producing a 50% inhibition of one unit of cdk4. Measurements were repeated at least in triplicate.

Identification of C5 by the Yeast Two-Hybrid System

Human cdk4 cDNA excised from pBAC/cdk4 at EcoRI and BamHI sites was gel-purified, and the cdk4 epitope library was constructed by random digestion of cdk4 cDNA with DNase I. DNA fragments of 200–300 bp were chosen and subcloned into pGAD424 vector. The library was transfected into *Saccharomyces cerevisiae* CG1945 harboring the pAS-MTS1/Δ1–8 vector expressing p16 N-terminally fused to the *GAL4* DNA binding domain. Cdk4 fragments were expressed in yeast from pGAD424 N-terminally fused to the *GAL4* activation domain. The library consisted of 7×10^4 independent clones expressed in the correct reading frame, which covered more than 99.99% of probability for representing all possible cdk4 fragments in this size range. The *HIS3* and *LacZ* genes in CG1945 under the control of *GAL1* transcription regulatory elements allowed CG1945 to grow on a histidine-deficient medium and acquire a blue color in the presence of X-gal, provided the cdk4 fragment binds to p16. The library was screened on a histidine-deficient medium. Grown colonies were subsequently screened for β-galactosidase activity using a filter assay as directed by the manufacturer (Boehringer Mannheim).

The colonies with the most intense blue color were chosen for further analyses. The yeast clones were relieved of the pAS-MTS1/Δ1–8 plasmid. The pGAD424 plasmids with cdk4 fragments were isolated from chosen clones and sequenced. These plasmids along with pAS-MTS1/Δ1–8 were cotransfected into another yeast strain *S. cerevisiae* SFY526, which is a construct expressing the N-terminal part of human lamine (from the plasmid pLAM5), a protein unrelated to and not interacting with cdk4 or p16, N-terminally fused to the *GAL4* DNA binding domain. pLAM5 was used as a negative control. The same hybrids were constructed with pGA-cdk4, a pGAD424 plasmid that expressed the full-length cdk4 fused to the C terminus of the GAL4 activation domain.

Pull-Down Assays for p16/C5 and p16/cdk4 Binding

Proteins were in vitro translated using the Single Tube Protein System 2 (Novagen) or TNT (Promega) and labeled with [^{35}S]-methionine. The proteins under study were mixed and incubated on ice for 30 min. The mixture was loaded onto a spin column containing the chromatographic resin and incubated on ice with shaking for 30 min. Then, the columns were centrifuged for 1 min at 5000 rpm and the resin was washed five times with the ice-cold buffer: GST pull-down buffer in the case of glutathione-Sepharose (20 mM Tris, 1 mM EDTA, 25 mM NaCl, 10% glycerol, 0.01% Nonidet P-40, 1 mM DTT, 0.2 mM AEBSF, 5 mg/ml aprotinin, 5 mg/ml leupeptin [pH 7.4 at room temperature]) or S-tag bind/wash buffer (20 mM Tris, 150 mM NaCl, 0.1% Triton-X 100, 1 mM DTT, 0.2 mM AEBSF, 5 mg/ml aprotinin, 5 mg/ml leupeptin [pH 7.5 at room temperature]). All manipulations were performed at 4°C. The proteins were eluted from the columns by boiling in 1× loading buffer, separated by SDS–PAGE on 15% tricine gel, and visualized by autoradiography. In the case of cotranslation, the DNAs of the plasmids encoding for the two proteins were mixed prior to in vitro transcription/translation (if the TNT kit was used), or they were transcribed individually and the mRNAs were mixed prior to in vitro translation (if Single Tube Protein System 2 was used).

The pCITE-p16/S plasmid used to generate p16 with the N-terminal S tag was constructed by subcloning human p16 cDNA from pET-MTS1 (Tevelev et al., 1996) into NcoI and BamHI sites of pCITE-4a (Novagen). N-terminally GST-fused p16 was produced using pTG-p16. N-terminally S-tag-fused cdk4 was produced using pCITE-cdk4/S, which was constructed by subcloning cdk4 cDNA from pAS-cdk4 into NcoI and SalI sites of pCITE-4a. The R24C mutant of cdk4, N-terminally fused to S-tag, was produced using pCITE-cdk4/S/R24C. pCITE-cdk4/S/R24C was constructed by subcloning mutated cdk4 cDNA from pTG-cdk4/R24C into NcoI and BamHI sites of pCITE-4a. The R24C mutant of C5 was constructed by replacing the BsrGI/PflMI fragment with the same oligonucleotides as for cdk4. It was further subcloned into pCITE-4a as described above.

Pull-Down Assay for p16-Binding to cdk4 Mutants

pCITE-cdk4 and pCITE-cdk4 mutants were used to produce wild-type cdk4 and cdk4 mutants, respectively. pCITE-cdk4/S, pCITE-cdk4 mutants, pCITE-p16/S, and pTG-p16 were used to produce wild-type cdk4 with S tag, cdk4 mutants with S-tag, p16 with S-tag, and GST-p16, respectively. pCITE-cdk4 was constructed by subcloning human cdk4 cDNA from pET-cdk4 into MscI and BamHI sites of pCITE-4a. pCITE-cdk4 mutants were constructed using the Quick Change kit (Stratagene).

Wild-type cdk4, cdk4 mutants, cdk4 with S tag, cdk4 mutants with S tag, and p16 with S tag were produced from the corresponding pCITE plasmids, and GST-p16 was produced from pTG-p16, using Single Tube System 2. 0.5 μg of DNA was used for individual expression of the corresponding cdk4 proteins. Each cdk4 mutant/S DNA was used to verify that equal amounts of each cdk4 mutant DNA produced almost equal amounts of cdk4 mutants in the in vitro expression system. For GST-p16 or S-p16 expression, multiple amounts of 0.5 μg of p16 DNA was in vitro translated in one tube, and aliquots of equal amounts of GST-p16 or S-p16 were used in p16-binding assays of cdk4 mutants.

The p16-binding assays of cdk4 mutants were performed in two sets of complementary experiments. The first set consisted of cdk4 mutants, S-tagged p16, and S-protein agarose beads (Novagen). The other set contained S-tagged cdk4 mutants, GST-p16, and S-protein agarose beads. In each set, individually in vitro expressed equal amounts of cdk4 mutants (or S-tagged cdk4 mutants) and aliquots of S-tagged p16 (or GST-p16) were mixed and incubated at 30°C for 30 min. The mixture was loaded onto a spin column containing 10 μl bed volume of S-protein agarose, and unbound proteins were removed as described in the previous section. Bound cdk4-p16/S or GST-p16-cdk4/S complexes were eluted by boiling the beads in SDS-gel loading buffer and separated by SDS–PAGE on a 12% polyacrylamide gel. cdk4 mutants (or cdk4/S mutants) and p16/S (or GST-p16) were detected by Western blotting with anti-cdk4 antibodies (Transduction Lab, #c18720) and anti-p16 antibodies (Santa Cruz, #sc-467), and by chemiluminescence detection system (Amersham, ECL detection).

GRAMM Calculations

GRAMM (Vakser and Aflalo, 1994) calculations were performed on an SGI O2 (180 MHz, R5000 processor) system using the following parameters: mmode = generic; eta = 1.5; ro = 30; fr = 0; crang = atom_radius; ccti = gray; crep = all; maxm = 1000; and ai = 10. For the C5 docking calculations, the first 58 amino acids of the cdk2 coordinates were used. The amino acids in this coordinate set were changed to match the amino acids in cdk4 using Insight II followed by energy minimization with Discover (Molecular Simulations, Inc.). These manipulations provided a new set of coordinates specifically for C5.

Acknowledgments

This is paper 2 in the series Tumor Suppressor p16^{INK4A}; for paper 1, see Tevelev et al. (1996). This work was supported by NIH Grant

CA69472 (to M.-D. T.) and by American Cancer Society Grant IRG16-33 (to I.-J. L. B.). The DMX-600 NMR spectrometer used was funded in part by NIH Grant RR08299 and NSF Grant BIR-9221639. Support from the Ohio Supercomputer Center is greatly acknowledged. Cdk2 coordinates were a gift from Professor Sung-Hou Kim. Human cyclin D2 cDNA was a generous gift from Dr. G. Peters. Human "large pocket" Rb cDNA corresponding to Rb amino acids 379–928 subcloned into pGEX was the generous gift of Dr. M. Ewen. The coordinates of p16 have been deposited in the Brookhaven Protein Data Bank.

Received December 31, 1997; revised January 20, 1998.

References

Baghdassarian, N., and Ffrench, M. (1996). Cyclin-dependent kinase inhibitors and hematological malignancies. Hematol. Cell Ther. *38*, 313–323.

Bax, A., and Davis, D.G. (1985). MLEV-17-based two-dimensional homonuclear magnetization transfer spectroscopy. J. Magn. Reson. *65*, 355–360.

Bork, P. (1993). Hundreds of ankyrin-like repeats in functionally diverse proteins: mobile modules that cross phyla horizontally? Proteins *17*, 363–374.

Brünger, A.T. (1992). X-PLOR, Version 3.1: a system for X-ray crystallography and NMR (New Haven and London: Yale University Press).

Coleman, K.G., Wautlet, B.S., Morrissey, D., Mulheron, J., Sedman, S.A., Brinkley, P., Price, S., and Webster, K.R. (1997). Identification of CDK4 sequences involved in cyclin D1 and p16 binding. J. Biol. Chem. *272*, 18869–18874.

Cordon-Cardo, C. (1995). Mutations of cell cycle regulators. Biological and clinical implications for human neoplasia. Am. J. Pathol. *147*, 545–560.

De Bondt, H.L., Rosenblatt, J., Jancarik, J., Jones, H.D., Morgan, D.O., and Kim, S.-H. (1993). Crystal structure of cyclin-dependent kinase 2. Nature *363*, 595–602.

Dyson, N. (1994). pRB, p107 and the regulation of the E2F transcription factor. J. Cell Sci. *18* (Suppl.), 81–87.

Fåhraeus, R., Paramio, J.M., Ball, K.L., Lain, S., and Lane, D.P. (1996). Inhibition of pRb phosphorylation and cell-cycle progression by a 20-residue peptide derived from p16CDKN2/INK4A. Curr. Biol. *6*, 84–91.

Fesik, A.W., and Zuiderweg, E.R.P. (1988). Heteronuclear 3D NMR spectroscopy. A strategy for the simplification of homonuclear 2D NMR spectra. J. Magn. Reson. *78*, 588–593.

Fueyo, J., Gomez-Manzano, C., Yung, W.K.A., Clayman, G.L., Liu, T.-J., Bruner, J., Levin, V.A., and Kyritsis, A.P. (1996). Adenovirus-mediated p16/CDKN2 gene transfer induces growth arrest and modifies the transformed phenotype of glioma cells. Oncogene *12*, 103–110.

Gorina, S., and Pavletich, N.P. (1996). Structure of the p53 tumor suppressor bound to the ankyrin and SH3 domains of 53BP2. Science *274*, 1001–1005.

Greenwald, I., and Rubin, G.M. (1992). Making a difference: the role of cell–cell interactions in establishing separate identities for equivalent cells. Cell *68*, 271–281.

Hanks, S.K. (1987). Homology probing: identification of cDNA clones encoding members of the protein-serine kinase family. Proc. Natl. Acad. Sci. USA *84*, 388–392.

Hannon, G.J., and Beach, D. (1994). $p15^{INK4B}$ is a potential effector of TGF-β-induced cell-cycle arrest. Nature *371*, 257–261.

Helps, N.R., Barker, H.M., Elledge, S.J., and Cohen, P.T. (1995). Protein phosphatase 1 interacts with p53BP2, a protein which binds to the tumour suppressor p53. FEBS Lett. *377*, 295–300.

Hirai, H., Suzuki, T., Fujisawa, J., Inoue, J., and Yoshida, M. (1994). Tax protein of human T-cell leukemia virus type I binds to the ankyrin motifs of inhibitory factor kappa B and induces nuclear translocation of transcription factor NF-κB proteins for transcriptional activation. Proc. Natl. Acad. Sci. USA *91*, 3584–3588.

Jin, X., Nguyen, D., Zhang, W.-W., Kyritsis, A.P., and Roth, J.A. (1995). Cell cycle arrest and inhibition of tumor cell proliferation by the $p16^{INK4}$ gene mediated by an adenovirus vector. Cancer Res. *55*, 3250–3253.

Kamb, A., Gruis, N., Weaver-Feldhaus, J., Liu, Q., Harshman, K., Tavigian, S., Stockert, E., Day, R., III, Johnson, B., and Skolnick, M. (1994). A cell cycle regulator potentially involved in genesis of many cell types. Science *264*, 436–440.

Kamijo, T., Zindy, F., Roussel, M.F., Quelle, D.E., Downing, J.R., Ashmun, R.A., Grosveld, G., and Sherr, C.J. (1997). Tumor suppression at the mouse *INK4a* locus mediated by the alternative reading frame product p19*ARF*. Cell *91*, 649–659.

Karadi, R., Billeter, M., and Wüthrich, K. (1996). Molmol: a program for display and analysis of macromolecular structures. J. Mol. Graphics *14*, 51–55.

Katchalski-Katzir, E., Shariv, I., Eisenstein, M., Friesem, A.A., Aflalo, A., and Vakser, I.A. (1992). Molecular surface recognition: Determination of geometric fit between proteins and their ligands by correlation techniques. Proc. Natl. Acad. Sci. USA. *89*, 2195–2199.

Koh, J., Enders, G.H., Dynlacht, B.D., and Harlow, E. (1995). Tumour-derived p16 alleles encoding proteins defective in cell-cycle inhibition. Nature *375*, 506–510.

Kouzarides, T. (1995). Transcriptional control by the retinoblastoma protein. Semin. Cancer Biol. *6*, 91–98.

Kuboniwa, H., Grzesiek, S., Delaglio, F., and Bax, A. (1994). Measurement of HN-Ha J couplings in calcium-free calmodulin using new 2D and 3D water-flip-back methods. J. Biomol. NMR *4*, 871–878.

Liu, Q., Neuhausen, S., McClure, M., Frye, C., Weaver-Feldhaus, J., Gruis, N.A., Eddington, K., Ullalunis-Turner, M.J., Skolnick, M.H., Fujimura, F.K., and Kamb, A. (1995). CDKN2 (MTS1) tumor suppressor gene mutations in human tumor cell lines. Oncogene *10*, 1061–1067.

Luh, F.Y., Archer, S.J., Domaille, P.J., Smith, B.O., Owen, D., Brotherton, D.H., Raine, A.R.C., Xu, X., Brizuela, L., et al. (1997). Structure of the cyclin-dependent kinase inhibitor $p19^{INK4D}$. Nature *389*, 999–1003.

Lux, S.E., John, K.M., and Bennett, V. (1990). Analysis of cDNA for human erythrocyte ankyrin indicates a repeated structure with homology to tissue-differentiation and cell-cycle control proteins. Nature *344*, 36–42.

Marion, D., Driscoll, P.C., Kay, L.E., Wingfield, P.T., Bax, A., Gronenborn, A.M., and Clore, G.M. (1989). Overcoming the overlap problem in the assignment of ^{1}H NMR spectra of larger proteins by use of three-dimensional heteronuclear ^{1}H-^{15}N Hartmann-Hahn multiple quantum coherence spectroscopy: application to interleukin 1β. Biochemistry *28*, 6150–6156.

Matsushime, H., Ewen, M., Strom, D.K., Kato, J.-Y., Hanks, S.K., Roussel, M.F., and Sherr, C.J. (1992). Identification and properties of an atypical catalytic subunit ($p34^{PSK-J3}$/cdk4) for mammalian D-type G1 cyclins. Cell *71*, 323–334.

Meijer, L., and Kim, S.-H. (1997). Chemical inhibitors of cyclin-dependent kinases. Meth. Enzymol. *283*, 117–118.

Miller, C.W., Yeon, C., Aslo, A., Mendoza, S., Aytac, U., and Koeffler, H.P. (1997). The $p19^{INK4D}$ cyclin dependent kinase inhibitor gene is altered in osteosarcoma. Oncogene *15*, 231–235.

Muhandiram, D.R., Xu, G.Y., and Kay, L.E. (1993). An enhanced-sensitivity pure absortion gradient 4D ^{15}N,^{13}C-edited NOESY experiment. J. Biomol. NMR *3*, 463–470.

Müller, R. (1995). Transcriptional regulation during the mammalian cell cycle. Trends Genet. *11*, 173–178.

Nilges, M., Clore, G.M., and Gronenborn, A.M. (1988). Determination of three-dimensional structures of proteins from interproton distance data by dynamical simulated annealing from a random array of atoms. FEBS Lett. *239*, 129–136.

Pace, C.N. (1986). Determination and analysis of urea and guanidine hydrochloride denaturation curves. Meth. Enzymol. *131*, 266–280.

Parry, D., and Peters, G. (1996). Temperature-sensitive mutants of $p16^{CDKN2}$ associated with familial melanoma. Mol. Cell. Biol. *16*, 3844–3852.

Russo, A.A., Jeffrey, P.D., Patten, A.K., Massagué, J., and Pavletich,

N.P. (1996). Crystal structure of the $p27^{Kip1}$ cyclin-dependent-kinase inhibitor bound to the cyclin A-cdk2 complex. Nature *382*, 325–331.

Sattler, M., Maurer, M., Schleucher, J., and Griesinger, C. (1995). A simultaneous ^{15}N,^{1}H- and ^{13}C,^{1}H-HSQC with sensitivity enhancement and a heteronuclear gradient echo. J. Biomol. NMR *5*, 97–102.

Serrano, M., Gómez-Lahoz, E., DePinho, R.A., Beach, D., and Bar-Sagi, D. (1995). Inhibition of ras-induced proliferation and cellular transformation by p16INK4. Science *267*, 249–252.

Serrano, M., Hannon, G.J., and Beach, D. (1993). A new regulatory motif in cell-cycle control causing specific inhibition of cyclin D/cdk4. Nature *366*, 704–707.

Serrano, M., Lee, H.-W., Chin, L., Cordon-Cardo, C., Beach, D., and DePinho, R.A. (1996). Role of the INK4a locus in tumor suppression and cell mortality. Cell *85*, 27–37.

Shapiro, G.I., Park, J.E., Edwards, C.D., Mao, L., Merlo, A., Sidransky, D., Ewen, M.E., and Rollins, B.J. (1995). Multiple mechanisms of $p16^{INK4A}$ inactivation in non-small cell lung cancer cell lines. Cancer Res. *55*, 6200–6209.

Sherr, C.J. (1996). Cancer cell cycles. Science *274*, 1672–1677.

Sklenar, V., Piotto, M., Leppik, R., Saudek, V. (1993). Gradient-tailored water suppression for ^{1}H-^{15}N HSQC experiments optimized to retain full sensitivity. J. Magn. Reson. A *102*, 241–245.

Suzuki, T., Kitao, S., Matsushime, H., and Yoshida, M. (1996). HTLV-1 Tax protein interacts with cyclin-dependent kinase inhibitor $p16^{INK4A}$ and counteracts its inhibitory activity towards CDK4. EMBO J. *15*, 1607–1614.

Suzuki-Takahashi, I., Kitagawa, M., Saijo, M., Higashi, H., Ogino, H., Matsumoto, H., Taya, Y., Nishimura, S., and Okuyama, A. (1995). The interactions of E2F with pRB and with p107 are regulated via the phosphorylation of pRB and p107 by a cyclin-dependent kinase. Oncogene *10*, 1691–1698.

Tevelev, A., Byeon, I.-J.L., Selby, T., Ericson, K., Kim, H.-J., Kraynov, V., and Tsai, M.-D. (1996). Tumor suppressor $p16^{INK4A}$: structural characterization of wild-type and mutant proteins by NMR and circular dichroism. Biochemistry *35*, 9475–9487.

Vakser, I.A., and Aflalo, C. (1994). Hydrophobic docking: a proposed enhancement to molecular recognition techniques. Prot. Struct. Funct. Genet. *20*, 320–329.

Vuister, G.W., Clore, G.M., Gronenborn, A.M., Powers, R., Garrett, D.S., Tshudin, R., and Bax, A. (1993). Increased resolution and improved spectral quality in four-dimensional $^{13}C/^{13}C$-separated HMQC-NOESY-HMQC spectra using pulsed field gradients. J. Magn. Reson. B *101*, 210–213.

Weinberg, R.A. (1995). The retinoblastoma protein and cell cycle control. Cell *81*, 323–330.

Whyte, P. (1995). The retinoblastoma protein and its relatives. Semin. Cancer Biol. *6*, 83–90.

Wölfel, T., Hauer, M., Schneider, J., Serrano, M., Wölfel, C., Klehmann-Hieb, E., De Plaen, E., Hankeln, T., Meyer zum Buschenfelde, K.-H., and Beach, D. (1995). A p16(INK4a)-insensitive CDK4 mutant targeted by cytolytic lymphocytes in a human melanoma. Science *269*, 1281–1284.

Zariwala, M., and Xiong, Y. (1996). Lack of mutation in the cyclin-dependent kinase inhibitor, $p19^{INK4D}$, in tumor-derived cell lines and primary tumors. Oncogene *13*, 2033–2038.

Zindy, F., Soares, H., Herzog, K.-H., Morgan, J., Sherr, C.J., and Roussel, M.F. (1997). Expression of INK4 inhibitors of cyclin-D kinases during mouse brain development. Cell Growth Differ. *8*, 1139–1150.